Electrochemistry Communications 139 (2022) 107307

Contents lists available at ScienceDirect

Electrochemistry Communications

journal homepage: www.elsevier.com/locate/elecom

The potential application of exfoliated MoS_2 to aqueous lithium-ion batteries

Nicholas David Schuppert [a], Santanu Mukherjee [c], Jacek B. Jasinski [b], Bijandra Kumar [d], Ayodeji Adeniran [a], Sam Park [a,*]

[a] Department of Mechanical Engineering, University of Louisville, KY 40292, USA
[b] Conn Center for Renewable Energy Research, University of Louisville, KY 40292, USA
[c] Swansea University, Singleton Park, Swansea, SA2 8PP, Wales, UK
[d] Elizabeth City State University, 1704 Weeksville Road, Elizabeth City, NC 27909

ARTICLE INFO

Keywords:
Aqueous lithium ion battery
Molybdenum disulfide
Renewable energy storage

ABSTRACT

Cost-effective storage remains one of the greatest challenges facing the adoption of renewable energy generation. Herein we present a cost-effective aqueous rechargeable battery based on MoS_2. Increased discharge capacities are achieved by liquid-phase exfoliation, resulting in a 105% increase in capacity and prolonged lithiation plateau. Contributing evidence is provided by High Resolution TEM investigation of the expanded van der Waals gap between adjacent MoS_2 layers and particle active surface area. Exfoliated MoS2 and a MoS_2/graphite composite cathode is also investigated, resulting in an increase of reversible lithiation levels over 3x that of the base exfoliated material. The preservation of discharge capacities and voltages indicates the composite is highly effective in improving reversible lithiation. Further examination of the cost-effectiveness of the composite reveals vastly superior storage-to-cost ratios relative to other ARB cathodes.

1. Introduction

Aqueous rechargeable batteries (ARBs) are a promising alternative to conventional lithium batteries for larger scale energy storage applications. Recent research in ARBs has shown improvements in fabrication costs and operational safety over lithium batteries yet do not compare in total storage [1–3]. Despite this, capacity deficiencies may be overcome with low cost electrode materials making cost competitive storage achievable. Numerous metal oxides [4], polyanionic compounds [5], and Prussian blue analogs [6–8] have been explored as cathodes for ARBs [9,10]. However, they have yet to result in large capacity, high retention, and low costs. More recently aqueous batteries utilizing phosphate-based cathodes have garnered attention due to their increased capacity and cycling stability, but possess sometimes costly or complicated fabrication procedures that inhibit the materials overall cost effectiveness [11,12]. Nano-structured cathodes utilized in zinc aqueous batteries have also captured much recent attention, resulting in high discharge capacities and long cycle life [13,14], but also suffer from more complicated or costly fabrication; MoS_2 is of particular interest in this regard. MoS_2 possesses high theoretical capacities relative to other ARB electrodes [15,16] and owing to its natural abundance it is uniquely positioned as a cost competitive alternative [17]. The application of MoS_2 as a cathode material for conventional lithium batteries has been the subject of considerable research in recent years due to the high storage potential (1200 mAh g^{-1}) and favorable lithiation its two dimensional layered structure[18,19]. However the low lithiation voltage of MoS_2 (~1.1 V) results in a battery of limited power and as such is one of the main detriments to utilizing MoS_2 in conventional cells [20]. Though considerable effort has been devoted to the study of MoS_2 in traditional lithium batteries utilizing organic electrolytes, up to this point no literature has been published on the application of MoS_2 to ARBs. While this is likely due to the low lithiation potential of MoS_2 vs. S.H.E., electrolysis of the aqueous electrolyte may be mitigated by appropriate choice of electrolyte salt and the use of electrode substrates with significant overpotential to hydrogen evolution.

Due to the limited stability window of all ARBs the low lithiation voltage of MoS_2 is less detrimental to performance than it might otherwise be in a traditional organic electrolyte [21]. Unfortunately a majority of MoS_2's reported discharge capacities are derived from lithium sulfide formation that occurs below 0.5 V and is irreversible

* Corresponding author.
E-mail address: Sam.Park@louisville.edu (S. Park).

https://doi.org/10.1016/j.elecom.2022.107307
Received 16 May 2022; Received in revised form 20 June 2022; Accepted 20 June 2022
Available online 27 June 2022

within the stability window of ARBs [18–20]. This redox couple is shown in Equ. 1 and 2.

$$Li_xMoS_2 + (4-x)e^- \rightarrow Mo + 2Li_2S\ (\ 0.6\,V\ vs.\ Li/Li^+) \quad (1)$$

$$S + 2Li^+ + 2e^- \rightleftarrows Mo + Li_2S\ (\ 2.2\,V\ vs.\ Li/Li^+) \quad (2)$$

Due to MoS_2's semiconducting nature, significant capacity fade attributed to irreversible lithiation occurs when discharging below 0.5 V, as lithiated Mo dissociates to form metallic Mo and Li_2S (Equ. 1) [20,22]. The ARBs cannot reversibly form Li_2S (Equ. 2) as charging to 2.2 V would likely lead to electrolysis of the aqueous electrolyte, and therefore will suffer from higher levels of capacity fade. MoS_2 is also a semiconductor and thus shows poor lithiation reversibility due to a relatively poor electronic conductivity, especially in the direction normal to the MoS_2 planes (poor layer-to-layer conductivity) [20].

A comparative study of the bulk and exfoliated MoS_2 materials is done both physically as well as electrochemically. Changes in electrochemical performance are related to particle active surface area and an expanded van der Waals gap between adjacent MoS_2 layers. Lithiation capacity (capacity due to the insertion and extraction of lithium ions) of MoS_2 and the formation of Li_2S is also examined with respect to the use of a conductive graphite additive (ex.MoS_2·GC). Lastly, the cost-effectiveness of the ex.MoS_2·GC is examined.

2. Experimental procedures

2.1 Material fabrication

MoS_2 powder (Sigma Aldrich) is suspended in isopropanol (IPA) and left as obtained (bulk MoS_2). Ex.MoS_2 is fabricated by suspending 300 mg of bulk MoS_2 powder in 60 ml of IPA, subjecting the mixture to probe sonication (25 W power) in a water bath for 36 h, centrifugation at 3000 rpm for 30 min and collecting/washing the supernatant with IPA. The ex.MoS_2·GC particles are fabricated by simple mixing of ex.MoS_2 supernatant and an excess suspension of graphite flake (Alfa Aesar, 99.8%) in IPA at 500 rpm for 1 h, resulting in a mass ratio 15:1 graphite to ex.MoS_2. Use of excess graphite insures that MoS_2 wetting in the composite is not limited by the available graphite surface. A 6 M $LiNO_3$ aqueous electrolyte is used due to its demonstrated high overpotential to electrolysis [21] and activated carbon (A.C., Kureha, ground by mortar and pestle and suspended in IPA) is the chosen anode material due to its low cost, high surface area (1200 $m^2\ g^{-1}$), and overpotential to electrolysis [23,24]. Excess anode mass is utilized to insure that MoS_2 is the capacity limiting material in all test cases. Cathode and anode fabrication was accomplished by drop casting each material suspension on conductive carbon paper substrates (Sigracet, 29 BC) and drying at 50 °C under atmospheric conditions between coatings.

2.2. Material characterization

SEM, XRD, Particle size analysis (PSA), Raman and UV/Vis spectroscopy was done to characterize the bulk and exfoliated materials; PSA was performed on homogenous IPA suspensions of bulk and ex.MoS_2. It should be noted that the PSA assumes spherical particle morphology. From Fig. 1A this morphology is known to be inaccurate and represents a limitation of the measurement. However relative comparisons between bulk and ex.MoS_2 particle size are useful to differentiate between the active surface areas of both materials. To do so we will define the active surface area to particle volume ratio (SVR) as.

$$SVR = \frac{\text{Surface Area}}{\text{Volume}} = \frac{4\pi r^2}{\frac{4}{3}\pi r^3} = \frac{6}{d}\ \mu m^{-1} \quad (3)$$

2.3. Electrochemical testing

Electrochemical testing of the varied MoS_2 cathodes was performed using full cells utilizing a 6 M $LiNO_3$ aqueous electrolyte and A.C. anode (excess mass) assembled in CR2032 coin cells under atmospheric conditions. Cutoff voltages of 0 V and 2 V, a specific current of 200 mA g^{-1} (5C). Reported capacities are calculated with respect to the mass of MoS_2 utilized.

2.4. Storage-to-cost ratio calculation

Storage-to-cost ratios presented are calculated using the reported 1st cycle discharge capacities and dividing by the approximate costs of the

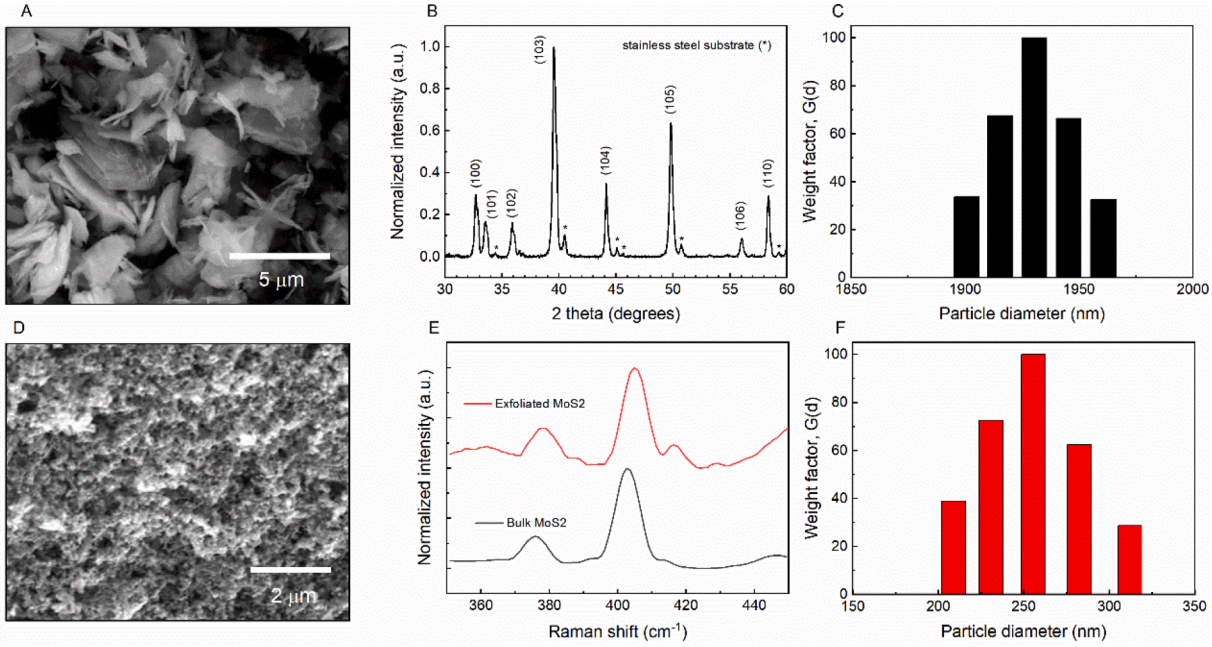

Fig. 1. SEM images of bulk and exfoliated MoS_2 particles conglomerates are shown in (A) and (D) respectively, with XRD of the bulk MoS_2 and important peaks indexed shown in (B). PSA distributions of the bulk and exfoliated MoS_2 particle conglomerations is shown in (C) and (F) respectively. Lastly, Raman spectra of the bulk and exfoliated MoS_2 particles is shown in (E).

reported cathodes. Material costs are gathered from Sigma Aldrich to provide a single reference point for comparison. A summary of discharge capacity, cycling stability and storage-to-cost ratio of commonly investigated ARB cathodes and the performance of the novel ex.MoS_2·GC cathode presented in this paper is shown in Table 1.

3. Results and discussion

SEM, XRD, PSA and Raman spectra of the bulk and exfoliated MoS_2 particle conglomerates is shown in Fig. 1. A comparison between the images shown in Fig. 1(A) and Fig. 1(D) highlights the extreme reduction in particle conglomeration size afforded by LPE. While the thin, flaky, layer-like structure of the bulk MoS_2 is readily apparent, the high alternating pressure of the sonication process has broken up the bulk particles and resulted in significantly smaller irregular conglomerations of exfoliated MoS_2 particles. The exfoliated MoS_2 particle conglomeration size has reduced to be indistinguishable at 2 μm. Indexed X-ray diffraction (XRD) peaks of the bulk MoS_2 (CCDC PDF card 00–002–0132 and 00–002–1133) confirm the as-obtained MoS_2 to be highly crystalline and phase-pure; background peaks of the stainless steel substrate used during testing have also been identified. Examination of the change in particle size shows the average particle diameter reduces from 1.9 μm to 254 nm after LPE, bringing with it a significant increase in active surface area, while the Raman spectra shown in Fig. 1(E) illustrates that no changes in chemical composition has occurred during the exfoliating process. A corresponding red-shift has occurred as a result of a reduction in layer number attributed to coulombic interactions between the layers of stacked MoS_2 sheets, and is in agreement with published literature [33]. From Equ. 3, the calculated SVR's of the bulk and exfoliated sample are found to be 3.1 μm^{-1} and 23.6 μm^{-1}, respectively. Thus LPE has resulted in a seven-fold increase in SVR over the bulk, thereby providing significantly improved access to intercalation sites during cell discharge.

High resolution TEM images (HRTEM) showing the layered structure of bulk and exfoliated MoS_2 is shown in Fig. 2(A) and (C) respectively and an image of the resulting IPA suspensions is shown in Fig. 2(B). After exfoliation a clear color transition takes place, changing from dark grey to a bright yellow. This is a result of MoS_2 transitioning from an indirect to direct bandgap material as the number of adjacent layers is reduced [34]. Ultraviolet–visible spectroscopy (UV/Vis) absorbance peaks of the bulk and ex.MoS_2 are shown in Fig. 2(D) to highlight this transition. All XRD, Raman, and UV/Vis data is in agreement with published literature [35–37]. The same High resolution TEM was used to examine any differences in the van der Waals gap between adjacent layers. An example of this measurement is shown in Fig. 2(E) with the collected data summarized in Table 2.

A reduction in layer number is observed of the ex.MoS_2 and is typical throughout. The van der Waals gap of the ex.MoS_2 was found to be 0.321 Å greater than that observed of the bulk, indicating that the reduction in layer number as a result of LPE has expanded the distance between adjacent planes. While this expansion is relatively small (~5% the initial gap), it is significant at the scale-length of the intercalating lithium ions. The expanded gap is equivalent to approximately 12% the diameter of the lithium atom and should provide significantly improved access to intercalation sites.

Table 1
Approx. costs, discharge capacities, cycling stabilities, and storage-to-cost ratio for cathodes of common ARB full cells and the ex.MoS_2·GC presented in this work [25–32].

Cathode material	Cost (USD per 25 g)	Initial capacity (mAh g^{-1})	Capacity after (n) cycles (mAh g^{-1})	Storage-to-cost ratio (mAh USD^{-1})
$LiFePO_4$ [29]	446.00 [26]	120	78 (10)	6.73
$LiMn_2O_4$ [32]	44.80 [27]	45	18 (25)	25.11
$LiMn_2O_4$ [30]	44.80 [27]	55.1	29.5 (100)	30.75
$LiCoO_2$ [31]	30.00 [25]	60	42 (12)	50.00
Ex.MoS_2	9.63 [28]	79.8	65.3 (50)	207.17

A comparison between the discharge results of the bulk and exfoliated materials are summarized in Fig. 3. An initial capacity of 61.9 mAh g^{-1} is observed of the bulk MoS_2 in Fig. 3(A), and owing to the lack of any clear discharge plateaus we may confidently say is that the bulk MoS_2 is a poor intercalating material. Changes in the discharge profile becomes more noticeable after the 10th cycle, as capacity from Li_2S formation becomes more pronounced and the lithiation capacity of the material structure deteriorates. After the 20th cycle the discharge profile of the bulk material has become entirely linear, indicating the loss of the small amount of lithiation-based capacity the material initially possessed and that any remaining capacity is likely due to lithium plating (similar to a capacitor). These observations are reinforced by the differential capacity vs voltage measurement shown in Fig. 3(B). There is very little indication of any lithiation based capacity owing to the lack of peaks observed near 1.1 V. Similarly, a new discharge peak develops *ca.* 0.3 V and is associated with the undesirable and irreversible formation of Li_2S.

These observations are in stark contrast to the exfoliated material results found in Fig. 3(D) and (E), where significant discharge plateaus and reduction peaks are observed. LPE of the MoS_2 has increased the initial discharge capacity of the material to 127.1 mAh g^{-1}, with considerably more pronounced plateaus *ca.* 1.1 V (lithiation-based capacity) and 0.3 V (lithium sulfide formation). More specifically the lithiation capacity of the ex.MoS_2 is significantly improved over the bulk, increasing from 34.5 mAh g^{-1} to 80.1 mAh g^{-1} within this voltage range. LPE has yielded a significant increase in lithiation capacity (plateau observed near 1 V) as well as below 0.5 V associated with Li_2S formation (*ca.* 0.3 V). This increase is attributed to two physical changes evoked by LPE; that a reduction in particle size has increased the SVR of the MoS_2 particles and as a result has increased the number of sites available for lithium intercalation and Li_2S formation [38]. Secondly, LPE has resulted in an expanded van der Waals gap that is especially significant on the scale of the intercalating species. This increased van der Waals gap between adjacent MoS_2 layers has improved access to interlayer space during lithiation. Additionally, large reduction peaks *ca.* 1.1 V and 0.3 V are clearly observable. The increased activity in both regions indicates that LPE of the material has drastically increased the lithiation-based capacity and the degree of Li_2S formation by providing greater access to lithium intercalation sites as well active sites for irreversible lithium sulfide formation. Similarly, the exfoliated sample rapidly loses electrochemical activity by the 10th and 20th discharge cycles but to an even greater degree than the bulk material. This is a direct consequence of the increased SVR and by extension, the active surface area of the ex.MoS_2.

Capacity retention vs cycling results shown in Fig. 3(C) confirm these observations. Both materials experience significant capacity fade as they approach *ca.* 40%, with the exfoliated sample experiencing the fastest levels of degradation. This is expected, as material degradation is often proportional to active surface area [39]. Severe lithiation capacity reduction observed within the first 20 cycles of the ex.MoS_2, as capacity within this region drops from 80.1 mAh g^{-1} to 20.8 mAh g^{-1} equivalent to a 74% reduction. Because this loss is observed most significantly within the intercalation region, it is attributed to irreversible lithiation as a result of MoS_2's low conductivity. The coulombic efficiency (C.E.) results of the bulk and exfoliated materials shown in Fig. 3(F) further reinforce these observations. Both materials possess initially low coulombic efficiency due to the excess carbon utilized as the anode, however both materials continue to show poor C.E. as they are cycled. While the exfoliated material performs much better than the bulk in this regard, it too shows high levels of irreversible lithiation and Li_2S formation.

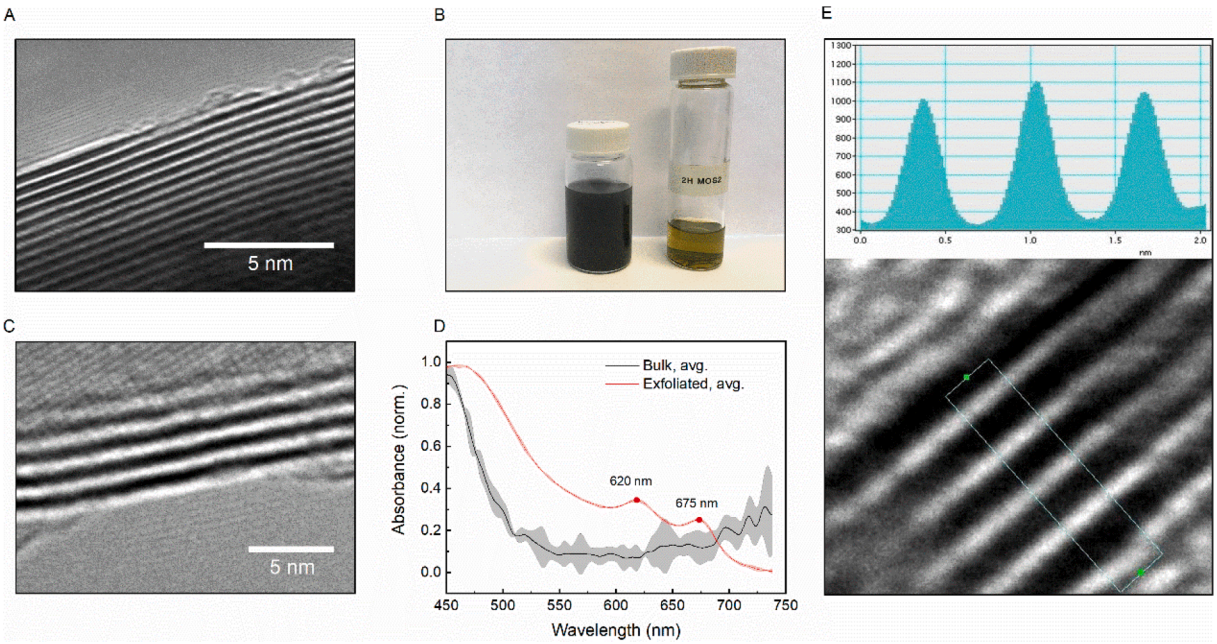

Fig. 2. HRTEM images of adjacent MoS_2 planes for (A) bulk and (C) exfoliated MoS_2 particles with 5 nm scale bars shown. (B) IPA suspensions of the bulk (left) and exfoliated MoS_2 particles highlighting the color transformation after LPE. (D) Average UV–vis spectra of the bulk and exfoliated materials and (E) example measurement of the van der Waals gap.

Table 2
Number of samples measured (N), mean interlayer spacing (μ), standard deviation (σ) and coefficient of variation (C_v) resulting from HRTEM analysis of bulk and ex.MoS_2 particles.

Material	N	μ (Å)	σ (Å)	C_v (%)
Bulk MoS_2	9	6.333	0.191	3.0
Ex.MoS_2	13	6.654	0.485	7.3

To improve upon the results obtained by LPE of the MoS_2, graphite particles are introduced to the exfoliated material, forming a more electronically conductive composite electrode. An SEM image of a characteristic ex.MoS_2·GC particle is shown in Fig. 4(A) with a pristine graphite particle shown inset. A change in surface roughness is readily apparent when comparing the two images, indicating that ex.MoS_2 has adhered to the smooth graphite surface.

Discharge voltage profiles versus capacity for the ex.MoS_2·GC material is shown in Fig. 4(B). A first cycle discharge capacity of 175.0 mAh g^{-1} is observed of the composite (not shown), however approximately 60 mAh g^{-1} of this capacity is obtained below 0.25 V and is due to lithium plating on the high-surface-area graphite particles [40,41]. To remove the influence of low voltage lithium plating on cell capacity and to examine effects afforded by conductive graphite on reversible lithiation, only capacities between 1.5 V and 0.5 V are shown in Fig. 4(B). Focusing in on this region allows for a more appropriate examination of the effect the graphite has on reversible lithiation in the composite. 1st and 50th cycle discharge capacities of 79.8 mAh g^{-1} and 65.3 mAh g^{-1} are observed of the composite material in this region. Relatively little lithiation capacity was sacrificed upon the addition of the conductive graphite, indicating that the presence of the graphite has had an extremely positive impact on levels of reversible lithiation and has not greatly restricted access to MoS_2 intercalation sites. Examination of Fig. 4(B) reveals that the majority of retention experienced by the ex.MoS_2·GC cathode occurs at voltages above 0.5 V, and thus the introduction of the conductive graphite to the ex.MoS_2 has resulted in significantly higher levels of reversible lithiation. The ex.MoS_2·GC electrode has experienced a relatively minor 11% reduction in capacity within the intercalation region after 20 cycles, and only 18% after 50 cycles. This represents a massive improvement over the cycling stability observed of the pure ex.MoS_2.

Capacity retention results for the composite material within the lithiation region and across the full tested voltage range is shown Fig. 4 (C) with retention results of the bulk and exfoliated materials shown superimposed for comparison. While all cell configurations experience a majority of their capacity fade within the first 10 discharge cycles and reach a steady state capacity by the 30th cycle, the ex.MoS_2·GC has retained its capacity to a significantly higher degree. The ex.MoS_2·GC cathode exhibits the highest degree of capacity retention, possessing 65% of its total initial capacity (112.3 mAh g^{-1}) and 82% of its lithiation capacity (65.3 mAh g^{-1}) by the 50th cycle. This indicates that the vast majority of capacity loss (77%) experienced by the ex.MoS_2·GC occurs as a result of irreversible Li_2S formation and not from irreversible lithiation. The ex.MoS_2·GC also displays superior coulombic efficiency (96%) when compared to the bulk and ex.MoS_2 cathodes, reaching a steady state efficiency higher than that observed of the other two batteries and in fewer cycles (10th cycle). The increased levels of capacity retention, storage efficiency and reversible lithiation observed of the composite over the ex.MoS_2 is attributed to the increased electrical conductivity of the composite afforded by the addition of the graphite particles. While the graphite additive was found to be very effective in reducing irreversible lithiation, it has done little to suppress Li_2S formation.

To examine how the ex.MoS_2·GC performs relative to other materials, a comparison of capacity, cycling stability and storage-to-cost ratio of commonly investigated ARB electrodes and the novel ex.MoS_2·GC cathode presented in this paper is shown in Fig. 4(E). With the exception of the $LiFePO_4$ cathode, the tested ex.MoS_2·GC cathode resulted in an ARB with initial discharge capacities significantly greater than the majority of ARB electrodes presented in Fig. 4(E) and Table 1, however the ex.MoS_2·GC electrode has retained its capacity to a much higher degree. In stark contrast to the 50th cycle lithiation retention rate of 82% observed of the ex.MoS_2·GC, the $LiFePO_4$ electrode (which possesses the highest initial capacity) retains only 65% of its capacity by only the 10th cycle. Additionally the ex.MoS_2·GC ARB is able to achieve a remarkably high storage-to-cost ratio of 207.17 mAh USD^{-1}, over 4x that of the next highest material.

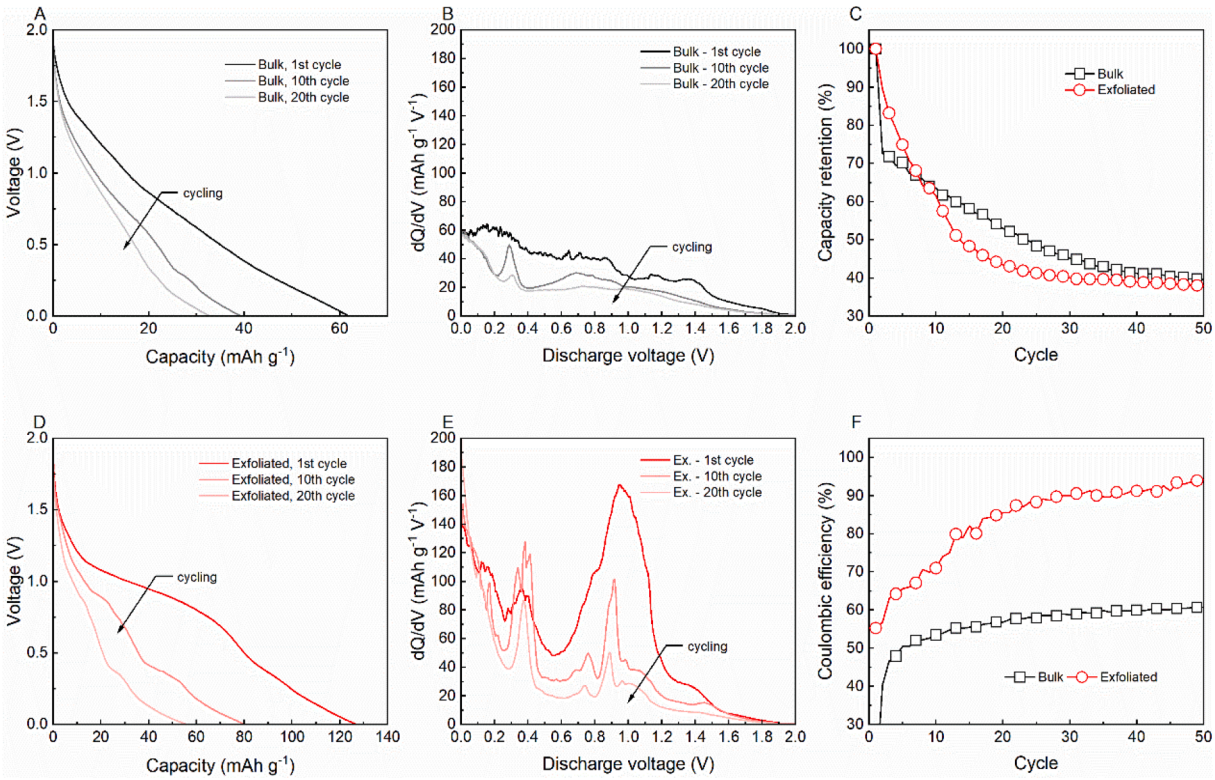

Fig. 3. Discharge voltage profiles versus specific capacity for the (A) bulk and (D) exfoliated MoS_2 materials. Differential capacity versus voltage highlighting all reduction peaks during cell discharge are shown in (B) for bulk MoS_2 and (E) ex.MoS_2. Discharge capacity and coulombic efficiency versus cycling number is shown for both materials in (C) and (F) respectively.

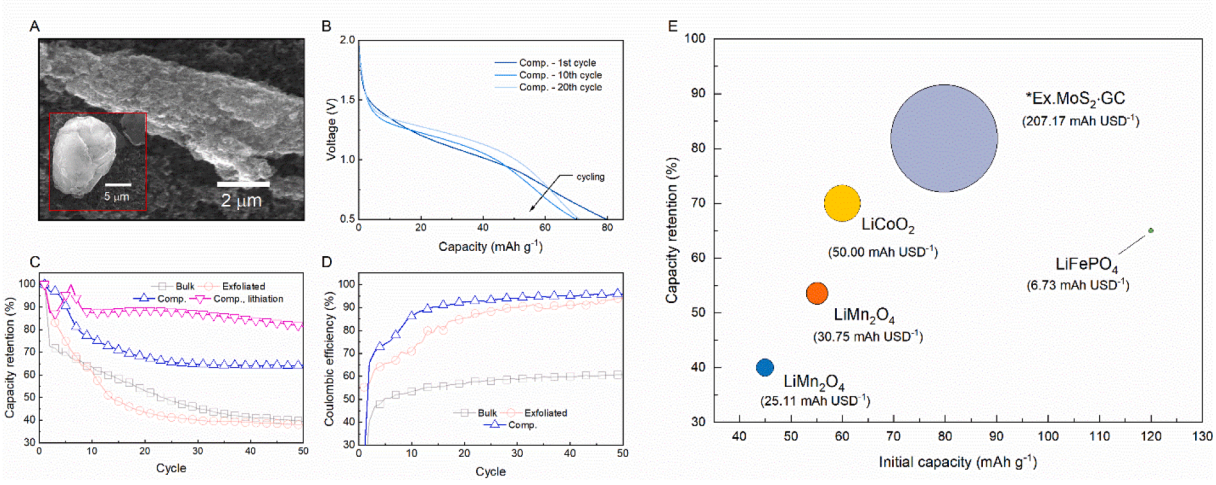

Fig. 4. A characteristic image of an ex.MoS_2·GC particle with a pristine graphite particle (inset, 5 µm scale bar) is shown in (A). Discharge profiles of the composite within the lithiation region of MoS_2 is shown in (B). Capacity retention results of the composite over the full tested voltage (blue) and just within the lithiation region (pink) are shown in (C) and coulombic efficiency results relative to the bulk and exfoliated materials is shown in (D). Discharge capacity, capacity retention and storage-to-cost ratios of the $LiCoO_2$ [25,31], $LiFePO_4$ [26,29], and $LiMn_2O_4$[27,30,32] and the ex.MoS_2·GC presented in this work [28] is shown in (E). Numerical values of approximate cost, discharge capacity, capacity retention and number of cycles run may be found in Table 1. (For interpretation of the references to color in this figure legend, the reader is referred to the web version of this article.)

4. Conclusions

LPE was effective in increasing accessibility to intercalation sites, thereby providing higher surface area to volume ratios and an expanded van der Waals gap. This was found to result in a significant increase in discharge capacity and protracted lithiation plateau over the bulk MoS_2 material. Significant improvements in capacity retention and coulombic efficiency were achieved by utilization of a conductive graphite additive, and was extremely effective in preserving reversible lithiation and the storage efficiency of ex.MoS_2, resulting in a remarkably superior storage-to-cost ratio. The tested ex.MoS_2·GC cathode has shown extremely promising results as a cost competitive material for ARBs, however before the material can be seriously considered additional work aimed at suppressing Li_2S formation is required.

CRediT authorship contribution statement

Nicholas David Schuppert: Conceptualization, Methodology, Investigation, Writing – review & editing. **Santanu Mukherjee:** Resources. **Jacek B. Jasinski:** Investigation. **Bijandra Kumar:** Resources. **Ayodeji Adeniran:** Resources. **Sam Park:** Writing – review & editing, Supervision, Visualization.

Declaration of Competing Interest

The authors declare that they have no known competing financial interests or personal relationships that could have appeared to influence the work reported in this paper.

Acknowledgements

The authors would like to thank the Conn Center for Renewable Energy at the University of Louisville for providing material characterization facilities. This work was supported by the NSF: IUCRC (EVSTS: # 1624712).

References

[1] N. Alias, A.A. Mohamad, J. Power Sources 274 (2015) 237–251.
[2] Q. Li, J. Chen, L. Fan, X. Kong, Y. Lu, Green Energy & Environment.
[3] Z. Li, L. Wang, K. Li, D. Xue, J. Alloy. Compd. 580 (2013) 592–597.
[4] H. Kim, J. Hong, K.-Y. Park, H. Kim, S.-W. Kim, K. Kang, Chemical Reviews, 114 (2014) 11788-11827.
[5] G. Rousse, J.M. Tarascon, Chem. Mater. 26 (2014) 394–406.
[6] M. Pasta, C.D. Wessells, N. Liu, J. Nelson, M.T. McDowell, R.A. Huggins, M. F. Toney, Y. Cui, Nat. Commun. 5 (2014) 3007.
[7] C.D. Wessells, R.A. Huggins, Y. Cui, Nat. Commun. 2 (2011) 550.
[8] C.D. Wessells, S.V. Peddada, M.T. McDowell, R.A. Huggins, Y. Cui, J. Electrochem. Soc. 159 (2011) A98–A103.
[9] M. Wu, J. Liao, L. Yu, R. Lv, P. Li, W. Sun, R. Tan, X. Duan, L. Zhang, F. Li, J. Kim, K.H. Shin, H. Seok Park, W. Zhang, Z. Guo, H. Wang, Y. Tang, G. Gorgolis, C. Galiotis, J. Ma, 15 (2020) 995-1013.
[10] J. Liao, W. Ni, C. Wang, J. Ma, Chem. Eng. J. 391 (2020), 123489.
[11] N. Nzimande, A. Haruna, P. Mwonga, B. Rasche, F. Cummings, K.I. Ozoemena, ACS Applied Energy Materials 4 (2021) 13085–13097.
[12] J. Zhao, Y. Li, X. Peng, S. Dong, J. Ma, G. Cui, L. Chen, Electrochem. Commun. 69 (2016) 6–10.
[13] Y. Zhao, Y. Wang, Z. Zhao, J. Zhao, T. Xin, N. Wang, J. Liu, Energy Storage Mater. 28 (2020) 64–72.
[14] Y. Li, Z. Huang, P.K. Kalambate, Y. Zhong, Z. Huang, M. Xie, Y. Shen, Y. Huang, Nano Energy 60 (2019) 752–759.
[15] Y.-C. Lu, B.M. Gallant, D.G. Kwabi, J.R. Harding, R.R. Mitchell, M.S. Whittingham, Y. Shao-Horn, Energy Environ. Sci. 6 (2013) 750–768.
[16] M. Wang, G. Li, H. Xu, Y. Qian, J. Yang, ACS Appl. Mater. Interfaces 5 (2013) 1003–1008.
[17] M.A. Lukowski, A.S. Daniel, F. Meng, A. Forticaux, L. Li, S. Jin, J. Am. Chem. Soc. 135 (2013) 10274–10277.
[18] C. Feng, J. Ma, H. Li, R. Zeng, Z. Guo, H. Liu, Mater. Res. Bull. 44 (2009) 1811–1815.
[19] Z. Yufei, W. Ye, Y. Jun, S. Wenhui, Y. Huiying, H. Wei, D. Xiaochen, 2D Materials 3 (2016), 024001.
[20] T. Stephenson, Z. Li, B. Olsen, D. Mitlin, Energy Environ. Sci. 7 (2014) 209–231.
[21] C. Wessells, R. Ruffo, R.A. Huggins, Y. Cui, Electrochem. Solid-State Lett. 13 (2010) A59–A61.
[22] X. Huang, Z. Zeng, H. Zhang, Chem. Soc. Rev. 42 (2013) 1934–1946.
[23] Q. Abbas, P. Ratajczak, P. Babuchowska, A.L. Comte, D. Bélanger, T. Brousse, F. Béguin, Journal of The Electrochemical Society, 162 (2015) A5148-A5157.
[24] X. Yan, Y. Jia, T. Odedairo, X. Zhao, Z. Jin, Z. Zhu, X. Yao, Chem. Commun. 52 (2016) 8156–8159.
[25] in, Sigma Aldrich, Price of LiCoO2, http://www.sigmaaldrich.com/catalog/product/aldrich/442704?lang=en&region=US, 2017.
[26] in, Sigma Aldrich, Price of LiFePO4, http://www.sigmaaldrich.com/catalog/product/aldrich/759546?lang=en&region=US, 2017.
[27] in, Sigma Aldrich, Price of LiMn2O4, http://www.sigmaaldrich.com/catalog/product/aldrich/482277?lang=en&region=US, 2017.
[28] in, Sigma Aldrich, Price of MoS2, http://www.sigmaaldrich.com/catalog/product/aldrich/234842?lang=en&region=US, 2017.
[29] P. He, J.-L. Liu, W.-J. Cui, J.-Y. Luo, Y.-Y. Xia, Electrochim. Acta 56 (2011) 2351–2357.
[30] G.J. Wang, H.P. Zhang, L.J. Fu, B. Wang, Y.P. Wu, Electrochem. Commun. 9 (2007) 1873–1876.
[31] G.J. Wang, N.H. Zhao, L.C. Yang, Y.P. Wu, H.Q. Wu, R. Holze, Electrochim. Acta 52 (2007) 4911–4915.
[32] H. Wang, K. Huang, Y. Zeng, S. Yang, L. Chen, Electrochim. Acta 52 (2007) 3280–3285.
[33] M. Baby, R. Kumar, J. Mater. Sci.: Mater. Electron. 29 (2018).
[34] X.D. Li, S.Q. Wu, Z.Z. Zhu, J. Mater. Chem. C 3 (2015) 9403–9411.
[35] H. Li, Q. Zhang, C.C.R. Yap, B.K. Tay, T.H.T. Edwin, A. Olivier, D. Baillargeat, Adv. Funct. Mater. 22 (2012) 1385–1390.
[36] A. O'Neill, U. Khan, J.N. Coleman, Chem. Mater. 24 (2012) 2414–2421.
[37] I. Song, C. Park, H.C. Choi, RSC Adv. 5 (2015) 7495–7514.
[38] F. Xiong, H. Wang, X. Liu, J. Sun, M. Brongersma, E. Pop, Y. Cui, Nano Lett. 15 (2015) 6777–6784.
[39] J. Xu, R.D. Deshpande, J. Pan, Y.-T. Cheng, V.S. Battaglia, Journal of The Electrochemical Society, 162 (2015) A2026-A2035.
[40] Z.X. Shu, R.S. McMillan, J.J. Murray, J. Electrochem. Soc. 140 (1993) 922–927.
[41] Y. Yamada, Y. Takazawa, K. Miyazaki, T. Abe, The Journal of Physical Chemistry C 114 (2010) 11680–11685.